JOC The Journal of Organic Chemistry

pubs.acs.org/joc Article

Triggering the Antitumor Activity of Acyclic Enediyne through Maleimide-Assisted Rearrangement and Cycloaromatization

Mengsi Zhang, Baojun Li, Huimin Chen, Haotian Lu, Hailong Ma, Xiaoyu Cheng, Wenbo Wang, Yue Wang, Yun Ding,* and Aiguo Hu*

Cite This: J. Org. Chem. 2020, 85, 9808−9819 Read Online

ACCESS | Metrics & More | Article Recommendations | Supporting Information

ABSTRACT: Acyclic enediynes are generally inactive under physiological conditions to be used as antitumor agents like their natural enediyne counterparts. A new mechanism named as maleimide-assisted rearrangement and cycloaromatization (MARACA) is uncovered to trigger the reactivity of acyclic enediynes. Through this mechanism, cascade 1,3-proton transfer processes are accelerated with the maleimide moiety at the ene position to enable the acyclic enediynes to undergo cycloaromatization and generate reactive radicals under physiological conditions. Computational studies suggest that the highest energy barrier for MARACA is 26.0 kcal/mol, much lower than that of Bergman cyclization pathway (39.6 kcal/mol). Experimental results show that maleimide-based enediynes exhibit low onset temperature, fast generation of radical species at 37 °C, and much faster reaction in aqueous solution than in nonpolar solvent, which is beneficial to achieve both high reactivity in physiological environment and high stability for storage and delivery in nonpolar media. The generated radical species are capable of causing high percentage of double-strand (ds) DNA cleavage, leading to significant cytotoxicity toward a panel of cancer cell lines with half inhibition concentration down to submicromolar level. Overall, the discovery of the MARACA mechanism provides a platform for designing novel acyclic enediynes with high potency for antitumor applications.

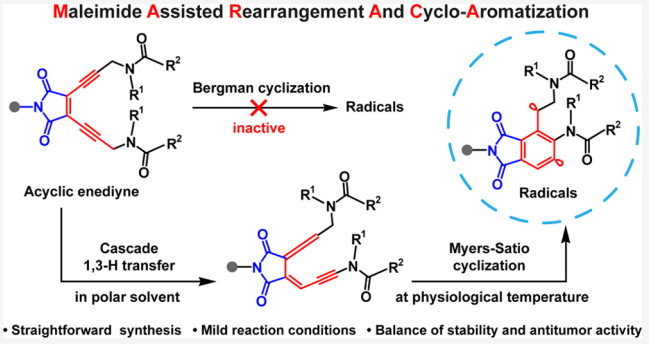

INTRODUCTION

Since their discovery in the 1980s, enediynes have become one of the most fascinating classes of natural products.[1] The unique enediyne architectures that prone to produce aromatic diradicals through the Bergman cyclization (BC)[2] endow these compounds with extremely high cytotoxicity against a broad range of cancer cells, leading to great potentials for the development of highly efficient antitumor agents. Indeed, one of the naturally occurring enediynes, calicheamicin, has been attached to monoclonal antibodies to form antibody−drug conjugates for clinical curing leukemia[3−5] and several others are undergoing preclinical evaluations.[6] Unfortunately, natural enediynes are difficult to prepare in good yield and preparation of the highly strained cyclic and complicated architecture of the unstable enediynes requires Herculean effort,[7−9] severely limiting their broader applications.[10] Employing synthetic enediynes in anticancer applications also constitutes significant difficulties.[11] The cyclic enediynes (especially those with small ring sizes) typically suffer difficulty in synthesis and short half-lives for derivatization or long-term storage, while the acyclic ones are generally inactive at physiological temperature.[12−14]

The Myers−Saito cyclization (MSC) of enyne-allene[15,16] is another type of thermal cycloaromatization besides BC that plays a fundamental role in the activation mode of natural enediyne antibiotics,[25,26] such as the chromophore of neocarzinostatin (NCS).[17] Both reactions share a significant similarity in producing highly reactive diradicals (or diradicaloids) from closed-shell compounds; however, MSC typically takes place at a much lower temperature. The decreased repulsion of in-plane π orbitals in the transoid orientation is believed to be the key for this facile and lower-activation-energy-demanding cycloaromatization.[18−21] Although some of the enyne-allene compounds have been isolated and characterized, due to their high reactivity, they were typically formed from stable precursors through various kinds of transformations. The sharp difference between the MSC reactivity of enyne-allene and the BC reactivity of acyclic enediyne provides a straightforward way for novel molecular design by taking advantage of cascade propargyl-allene rearrangements and thermal cycloaromatization. Many efforts have been devoted to facilitate this kind of transformation in

Received: May 9, 2020
Published: July 13, 2020

https://dx.doi.org/10.1021/acs.joc.0c01124
J. Org. Chem. 2020, 85, 9808−9819

Scheme 1. Synthesis of Two Model Enediyne Compounds and Schematic Illustration of Formation of Compound 3 from EDY-B: (a) $(PPh_3)_2PdCl_2$, CuI, *n*-$BuNH_2$, Tetrahydrofuran (THF), r.t., 18 h; (b) $(PPh_3)_2PdCl_2$, CuI, *N*,*N*-Diisopropylethylamine (DIPEA), Toluene/THF, r.t., 12 h

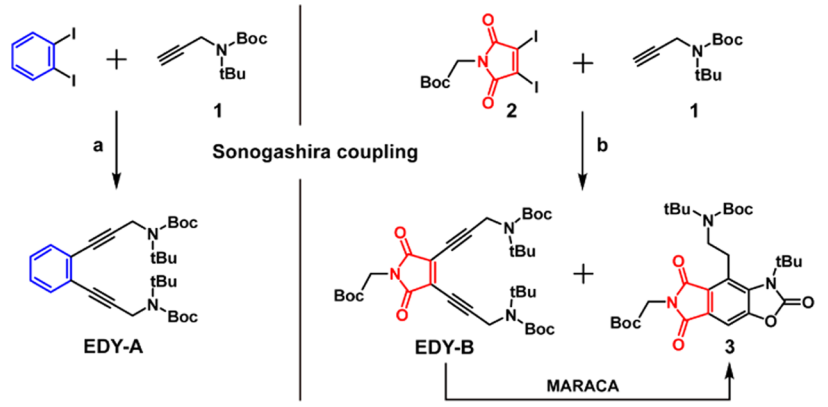

Scheme 2. Schematic Illustration of the Proposed MARACA Mechanism[a]

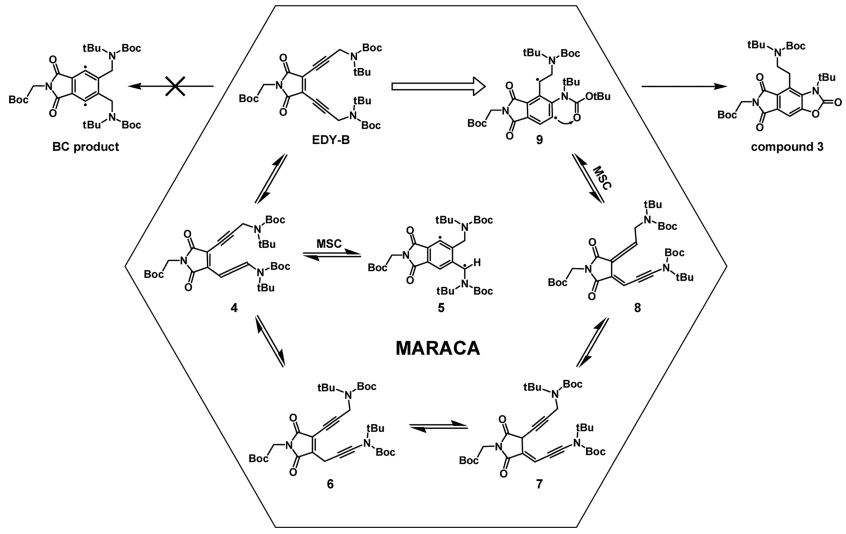

[a]The formation of compound 3 and the unlikely formation of BC product are presented as well.

the presence of an acid, base, oxidant, and transition-metal complex or under high temperature.[2,22−27] However, most of these conditions do not resemble biological systems.

In pursuit of uncovering the antitumor potencies of acyclic enediynes, we recently found that several kinds of acyclic enediyne compounds exhibited unprecedented high reactivity to generate radical species under relatively mild conditions.[28−32] All of these enediyne compounds share the same functionality at the ene position, maleimide. The maleimide moiety was first found to play an important role in lowering the onset temperature of cycloaromatization.[28] Later on, we found that when the steric and electronic properties of the substituents at the alkyne termini were finely tuned, the highly reactive acyclic enediynes were able to produce radical species under physiological conditions.[29−32] The energy barriers however were comparable to or even higher than those of the nonreactive acyclic enediynes if calculated through BC pathways (close to 40 kcal/mol),[33] implying the possibility of a new mechanism involved. To this end, we herein report in-depth investigations on this kind of intriguing reactions. We confirmed that the facile cycloaromatization of the acyclic enediynes with maleimide moieties originated from a "maleimide-assisted rearrangement and cycloaromatization" mechanism (abbreviated as MARACA). The propargyl-allene tautomerization was greatly facilitated by maleimide group to enable the otherwise nonreactive acyclic enediynes to undergo MSC in physiologically relevant environments. Following this line, several acyclic enediynes were designed and synthesized. They were stable in nonpolar solvents but quickly generated radical species in aqueous solutions to cause a high percentage of double-strand (ds) DNA cleavage and lead to apoptosis of tumor cells at submicromolar concentrations.

RESULTS AND DISCUSSION

Synthesis of Model Enediynes. To clarify the unique role of maleimide moiety in the cyclization of enediynes, two model compounds equipped with the same alkyne functionalities were designed. **EDY-A** features a benzene group at the ene position, representing common acyclic enediynes,[34−39] while **EDY-B** features a maleimide group at the same position. The two *tert*-butyl groups of different types were installed in the terminal alkyne, *tert*-butyl *tert*-butyl(prop-2-yn-1-yl)-carbamate (**1**), as chemical shift indicators for nuclear magnetic resonance (NMR) analysis. Another kind of *tert*-

https://dx.doi.org/10.1021/acs.joc.0c01124
J. Org. Chem. 2020, 85, 9808−9819

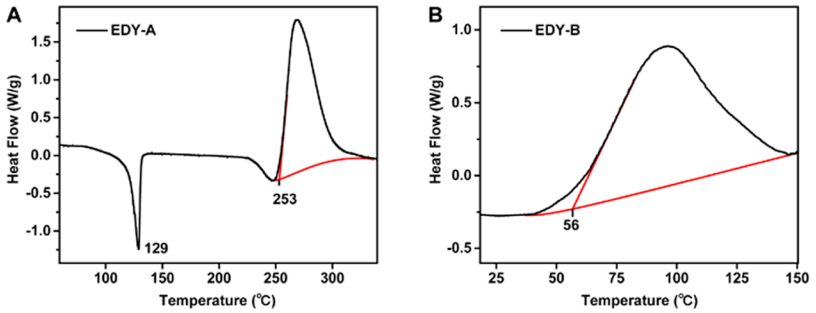

Figure 1. DSC curves of **EDY-A** and **EDY-B**. The baselines are marked in red to guide the eye.

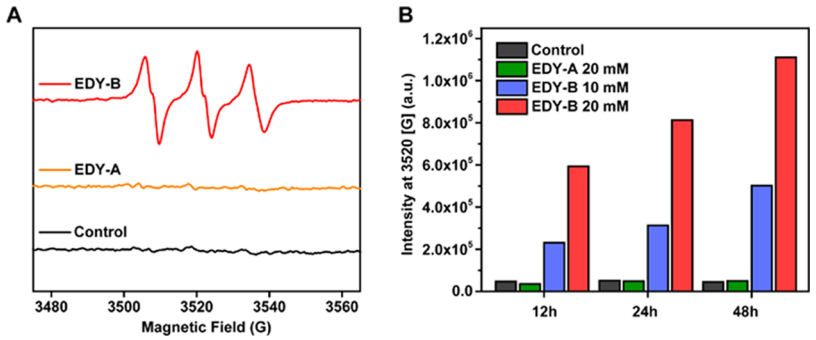

Figure 2. (A) EPR spectra of control, **EDY-A** (20 mM), and **EDY-B** (20 mM) in the presence of PBN (100 mM) in DCE at 37 °C for 12 h. (B) Time-dependent EPR signal intensities at 3520 G of control, **EDY-A** (20 mM), and **EDY-B** (10 and 20 mM) in the presence of PBN (100 mM) in DCE at 37 °C for 12, 24, and 48 h, respectively.

butyl group was installed in the maleimide moiety (**2**) for the same reason. Compounds **1**[40] and **2**[41] were synthesized according to literature procedures, while 1,2-diiodobenzene was obtained from a commercial resource. The Sonogashira coupling reaction between alkyne **1** and 1,2-diiodobenzene proceeded smoothly to produce **EDY-A** in good yield at room temperature (Scheme 1). Interestingly, when the similar experimental procedure was subjected to the Sonogashira coupling reaction between alkyne **1** and compound **2**, **EDY-B** was not isolated as the only product. Compound **3** with distinct bright blue fluorescence was isolated in a comparable yield to **EDY-B**. Moreover, the transformation of **EDY-B** to compound **3** was clearly observed with a prolonged reaction time or at an elevated reaction temperature, suggesting the possibility of converting **EDY-B** to compound **3** in the reaction mixture. Indeed, when pure **EDY-B** was heated in methanol, compound **3** was also obtained together with some polymeric products. The molecular structures of two enediynes were confirmed with NMR and high-resolution mass spectrometry (HR-MS) analyses (Supporting Information). The structure of compound **3** was characterized by 2D NMR, HR-MS, and single-crystal X-ray diffraction analyses (Supporting Information). The sharp difference between the molecular structures of compound **3** and the possible BC product (see Scheme 2) unambiguously indicates the involvement of rearrangement and ring closure reactions, suggesting that a new reaction mechanism hides behind the cyclization of maleimide-based **EDY-B**.

Thermal Reactivity of EDY-A and EDY-B. The thermal reactivities of two model enediyne compounds were investigated with differential scanning calorimetry (DSC) analysis. This method allows recording the onset temperature of thermal cyclizations of enediynes and enyne-allenes over a range of temperatures.[42,43] As shown in Figure 1, **EDY-A** holds a sharp endothermal melting peak at 129 °C, followed by an exothermal peak at 253 °C, which corresponds to the polymerization of free-radical intermediates[44] formed from cycloaromatization of enediynes. Basak et al. demonstrated that a series of structurally similar acyclic enediyne possessed high onset temperatures, typically beyond 200 °C, attributing to BC mode.[45] In contrast, **EDY-B** reveals a very low onset temperature at 56 °C, much closer to physiological temperature and nearly 200 °C lower than that of **EDY-A** despite bearing the identical alkyne functionalities. The computed activation barriers for **EDY-A** and **EDY-B** through BC pathway are almost the same, close to 40 kcal/mol (Figure S1), which fits well with the low thermal reactivity of **EDY-A**, but clearly has a discrepancy with the facile reaction of **EDY-B**. Therefore, we can conclude that when maleimide moiety is installed at the ene position of an enediyne compound, a new pathway with much lower activation barrier is created, leading to a much faster reaction at low temperature. Taking the fact that compound **3** is formed from **EDY-B** into consideration, rearrangement reactions are also involved in this new pathway and they are facilitated by the maleimide moiety as well. Altogether, a new mechanism named as MARACA is believed to guide the cyclization of **EDY-B** and other kinds of maleimide-based enediynes to enable them to generate reactive radical species at a low temperature for antitumor applications as discussed below.

Detection of Radical Intermediates. The possibility of generating free radicals from enediynes was verified using electron paramagnetic resonance (EPR) spectroscopy.[46] In general, it is difficult to monitor the transient radical intermediates formed from cycloaromatization due to their very low equilibrium concentration relative to that of enediynes.[47,48] Thus, a spin trap, *N-tert*-butyl-α-phenylnitrone (PBN), was exploited to capture the short-lived radicals by

https://dx.doi.org/10.1021/acs.joc.0c01124
J. Org. Chem. 2020, 85, 9808−9819

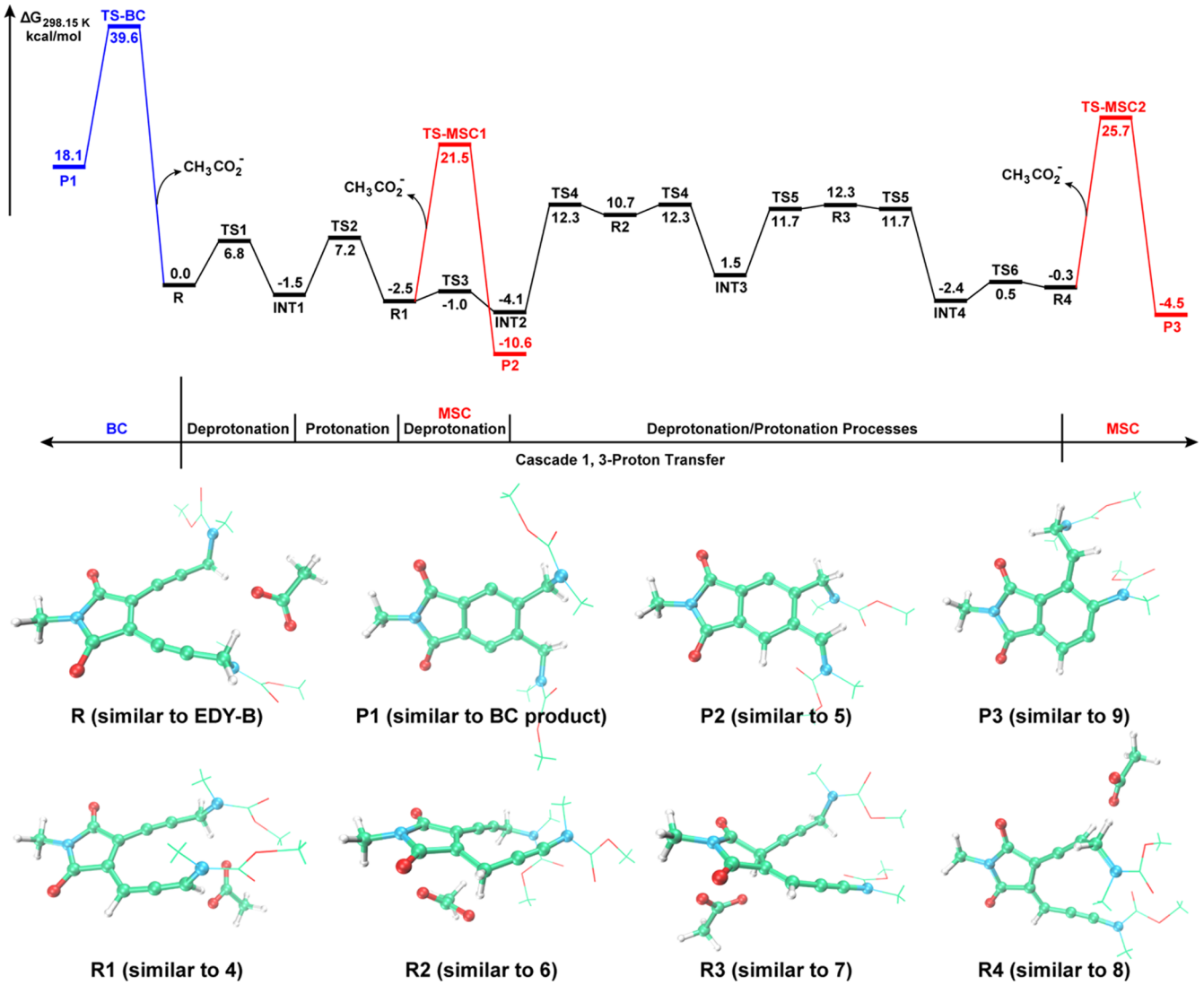

Figure 3. DFT computed Gibbs free-energy profile (kcal/mol) for BC (blue lines), cascade 1,3-proton transfer in the presence of acetate anion (black lines), and MSC (red lines) pathways of model enediyne **R** calculated at the (U)B3LYP/6-31G(d) level. Optimized structures of selected important stationary points in the potential energy surface shown below. Color code: C, green; O, red; N, blue; H, white. The rest of the structures can be found in the Supporting Information.

converting them into stable radical adducts.[49,50] **EDY-A** and **EDY-B** were dissolved in 1,2-dichloroethane (DCE) in the presence of excess PBN, respectively, then kept at 37 °C for 12, 24, and 48 h for the EPR studies. As shown in Figure 2A, the spin-trapped PBN adducts with a typical triplet peak is observed with **EDY-B**, uncovering the generation of radicals that probably originate from the smooth cycloaromatization at a physiological temperature. Figure 2B shows that the intensity of the recorded signals for **EDY-B** at 3520 G increases in both time- and concentration-dependent manners. In contrast, the EPR measurement of **EDY-A** shows a negligible signal, consistent with its high BC onset temperature and extremely low reactivity at 37 °C. The maleimide-assisted formation of the reactive radical species is of critical importance for the biological activity of maleimide-based enediynes.

General Scheme of MARACA. According to the above findings, the two model enediynes exhibit striking differences in thermal reactivity and the performance of free-radical generation, which is related to the fact that **EDY-A** undergoes BC mode, while **EDY-B** goes through a different pathway. A new mechanism thus is proposed after careful comparison of the molecular structures of compound **3** and its precursor **EDY-B**, involving cascade rearrangements and cycloaromatization, as shown in Scheme 2. The first step in this multistep transformation is the tautomerization of one of the propargyl groups to form an enyne-allene isomer **4**, which is known as an MSC precursor to produce the α,3-didehydrotoluene diradical **5**. On the other hand, a similar enyne-allene intermediate **8** is formed starting from **4** via further 1,3-proton transfer processes, which proceeds through another MSC to give diradical **9**. The aryl radical in **9** immediately undergoes 5-endo ring closure/radical cyclization and subsequent hydrogen abstraction to afford compound **3**, which is considered as a thermodynamically favored product. The proposed MARACA mechanism is verified by means of density functional theory, where the calculated energy barriers suggest that the rearrangement and cyclization processes of enediynes are feasible at room temperature (see below). It is noteworthy that although the conversion of **EDY-B** to compound **3** was achieved at 37 °C in methanol without any additive, the

https://dx.doi.org/10.1021/acs.joc.0c01124
J. Org. Chem. 2020, 85, 9808−9819

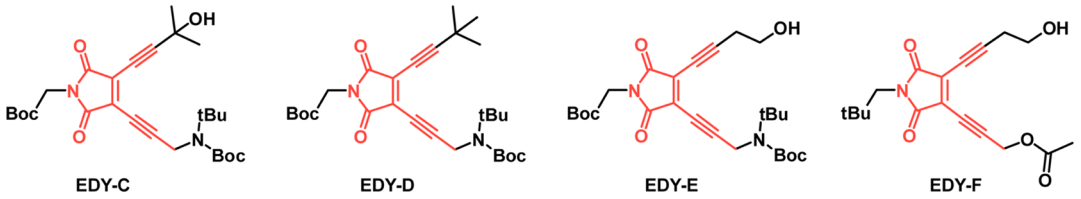

Figure 4. Molecular structures of **EDY-C**, **D**, **E**, **F**.

addition of a trace amount of weak base like triethylamine or sodium acetate indeed accelerated this transformation. On the contrary, **EDY-A** was stable at 37 °C even in the presence of excess strong base like 1,8-diazabicyclo[5.4.0]undec-7-ene. In other words, when enediynes are exposed to physiologically relevant environments, the presence of maleimide group is essential to facilitate the isomerization, driving enediynes away from the one-step BC mechanism and directing them to multistep rearrangements and MSC reaction, triggering the free-radical generation ability of acyclic enediynes at low temperature.

Computational Study. To understand the preference of **EDY-B** reacting through cascade rearrangements and cyclo-aromatization to generate compound **3** rather than BC product, the reaction mechanism was investigated in detail with structurally simplified models (the structures of these models are shown in Figure 3 and Scheme S1). Acetate anion, acting as the proton shuttle, was chosen to accomplish the reaction pathways when proton transfers were involved in the rearrangement reactions. Density functional theory (DFT)[51,52] studies have been carried out with Gaussian 09 program[53] using the (U)B3LYP exchange and correlation functional and the 6-31G(d) basis set in gas phase. A restricted approach was employed during geometry optimizations for the closed-shell structures, while for the optimizations of the transition states (TS) of the BC, MSC, and the biradical products, an unrestricted broken-symmetry ansatz has been utilized. This computational setup has been successfully applied in the mechanistic studies of rearrangement and cyclization reactions.[33,45] Harmonic vibration frequency calculations were carried out at 298.15 K, and the optimized structures are all shown to be either minima (with no imaginary frequency) or TSs (with only one imaginary frequency). Intrinsic reaction coordinate (IRC) calculations were performed to confirm the connection of each TS to its corresponding reactant and product. For each hydrogen transfer intermediate connecting two adjacent TSs, structure optimizations are carried out based on both IRC calculations, where the configuration with lower Gibbs free energy is chosen to represent the intermediate.

As shown in Figure 3, an extremely high activation energy for BC of the acyclic enediyne **R** is obtained, at 39.6 kcal/mol. Such a high barrier requires a high temperature (over 200 °C) to trigger this reaction, which is unfavorable for the application in biological systems. Alternatively, a low-energy-demanding route to generate diradical products arises, involving isomerization through 1,3-proton transfer assisted by acetate anion and subsequent MSC. Over **TS1** (6.8 kcal/mol), the propargyl proton of **R** is abstracted by the acetate anion, leading to the intermediate **INT1**. Subsequently, the protonation of alkynyl carbon occurs to yield the enyne-allene **R1** over a barrier of 8.7 kcal/mol. The MSC of **R1** might take place to generate diradical **P2** via **TS-MSC1** with the activation energy of 24.0 kcal/mol. These results clearly reveal the preference of MSC over BC if the rearrangement reaction is achieved under mild conditions. The isomerization of **R1** may continue with further 1,3-proton transfer to yield retro-propargyl **R2** via deprotonation and protonation processes with the barrier of 1.5 and 16.4 kcal/mol, respectively, corresponding to **TS3** and **TS4**. With two more 1,3-proton transfer steps, a second enyne-allene **R4** is formed. At this point, the diradical **P3** is generated through MSC over **TS-MSC2** (26.0 kcal/mol). Throughout this MARACA mechanism, the MSC steps are the rate-limiting steps, while the proton transfer steps are all with low energy barriers, and even a very weak base may act as an efficient proton shuttle in the 1,3-proton transfer processes. In comparison to much high barriers of 1,3-proton shifts observed by Alabugin et al.,[54] the dramatic acceleration of the propargyl-allenyl rearrangement by maleimide moiety clearly stands out. In addition, it is noteworthy that the first diradical **P2** is calculated to lie 8.1 kcal/mol below enyne-allene **R1** in Gibbs free energy, while the latter diradical **P3** is calculated to be exothermic by only 4.2 kcal/mol compared to **R4**. Meanwhile, the facile 5-endo attack of phenyl radical in **9** (similar to **P3**) to the *t*-Boc group allows the formation of thermodynamically stable compound **3**, as found in our experiments (Scheme 1). Combining the experimental and computational findings, it is unambiguously confirmed that the presence of the maleimide group enables acyclic enediynes to transform into reactive enyne-allenes via one- or multistep rearrangement and undergo MSC in physiologically relevant environments through the MARACA mechanism.

Synthesis of Maleimide-Based Enediyne Derivatives. According to the above findings, only one propargyl structure in the enediyne core is needed to realize the desired MARACA mechanism for maleimide-based enediynes. Therefore, we rationally designed and synthesized four more enediynes in view of three adjustable sites, the one propargyl group necessary for rearrangement reaction, the substituents at maleimide moiety, and the other alkyne both ready for modulating the log*P* value regarding the quantitative estimate of drug-likeness (QED).[55] The structures of these enediynes (Figure 4) have been characterized by NMR and HR-MS analyses. DSC study showed that these enediynes had similar onset temperatures ranging from 56 to 70 °C (Figure S3 and Table S1), implying similar thermal reactivity to **EDY-B** at a physiological temperature for antitumor applications.

Solution-Phase Reactivity of Enediynes. The chemically synthesized enediynes typically face the dilemma of high reactivity in antitumor application and low stability for long-term storage or derivatization since cycloaromatizations like BC and MSC are intramolecular processes and are insensitive to their environments.[56] Encouragingly, the MARACA mechanism provides a solution to this issue as the 1,3-proton shift exhibits significant solvent polarity dependence.[57−59] To investigate the effect of solvent polarity on their reactivity, **EDY-F** that has considerable solubility in both organic and aqueous solutions for facile UV−vis spectroscopic study was chosen as a model enediyne. Pure water and DCE were

https://dx.doi.org/10.1021/acs.joc.0c01124
J. Org. Chem. 2020, 85, 9808−9819

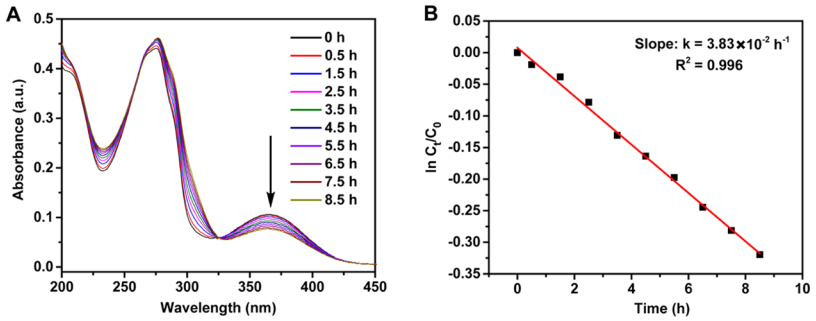

Figure 5. (A) UV−vis absorption spectral changes of **EDY-F** (10^{-4} M) in water. (B) Solution-phase kinetic plots for **EDY-F** in water at 365 nm.

selected to represent polar and nonpolar media, respectively. Solution-phase kinetic experiments were conducted at 37 ± 0.1 °C, and the concentration changes of **EDY-F** were monitored with UV−vis spectroscopy. The clear decrease of absorption intensity at 365 nm for **EDY-F** has been observed within 9 h in aqueous solution (Figure 5A). Accordingly, the absorbance representative of concentration versus time is plotted (Figure 5B), which shows a first-order reaction kinetics with a rate constant (k) of 3.83×10^{-2} h^{-1} and half-life of 18 h, a balanced reactivity and stability for biological applications.[60,61] Interestingly, the situation in DCE solution is entirely different with extremely slow changes in the concentration of **EDY-F** for the initial 12 h (Figure S4), corresponding to a half-life of nearly 2 months. Such a huge difference of reactivity in two kinds of solvents stresses that the stability of enediynes largely depends on the solvent polarity that dictates the propargyl-allenyl rearrangement, providing a promising strategy to balance the reactivity and stability for acyclic enediynes, i.e., to proceed the derivation, storage, and drug delivery in nonpolar media and to exert their high reactivity in physiological environments, rendering the potential application as clinical drugs.

DNA Cleavage Activity of Enediynes. One crucial feature of enediynes is their ability to abstract H atoms from the deoxyribose backbone and cause DNA cleavage. For natural enediynes, even at low concentrations, they can significantly lead to double-strand (ds) DNA cleavage.[62] The ds DNA cleavage mode, which is much more difficult for cells to repair than the single-strand (ss) DNA cleavage, can culminate in efficient self-programmed cell death (apoptosis), achieving the high cytotoxicity to tumor cells for chemotherapy. For example, calicheamicin possessed 25% of ds DNA cleavage (~1:3 ds/ss ratio)[63] and a similar ds/ss ratio (1:5) was found with NCS,[64] attributing to their outstanding antitumor performance. For the maleimide-based enediynes, highly reactive diradicals are generated through the MARACA mechanism, endowing them with DNA cleavage ability. To this end, **EDY-C** and **EDY-F** were selected to evaluate their DNA cleavage performance and agarose gel electrophoresis experiments were carried out to differentiate DNA in supercoiled circular (Form I), circular (Form II), and linear (Form III) forms or even fragments (Figure 6A). pUC19 plasmid DNA were incubated with varied concentrations of **EDY-C** or **EDY-F** at 37 °C for 48 h, respectively, and the relative amounts of the three DNA forms (Figure 6B) were analyzed with densitometric analysis on the stained electrophoretic images. As the concentration of **EDY-C** or **EDY-F** increases, a decrease of Form I (and even Form II) and a concurrent increase of Form III of pUC19 are observed. The high percentage of ds DNA cleavage (Figure 6C) originates from binding of

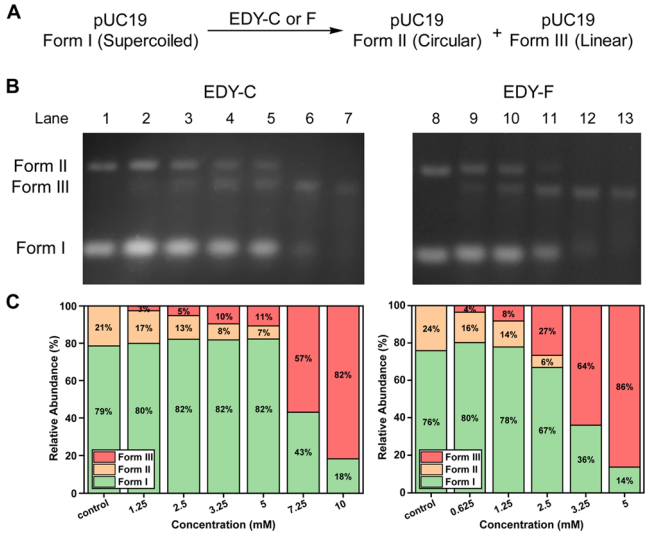

Figure 6. (A) Schematic presentation of the DNA cleavage activity of **EDY-C** and **EDY-F**. Agarose gel electrophoretic images (B) and quantified cleavage data (C) for DNA cleavage assay. Lane 1 and Lane 8: pUC19 (10 μg/mL) alone; Lane 2 to Lane 7: pUC19 (10 μg/mL) was incubated with 1.25 mM (Lane 2), 2.5 mM (Lane 3), 3.25 mM (Lane 4), 5 mM (Lane 5), 7.25 mM (Lane 6), and 10 mM (Lane 7) of **EDY-C** at 37 °C for 48 h; Lane 9 to Lane 13: pUC19 (10 μg/mL) was incubated with 0.625 mM (Lane 9), 1.25 mM (Lane 10), 2.5 mM (Lane 11), 3.25 mM (Lane 12), and 5 mM (Lane 13) of **EDY-F** at 37 °C for 48 h. Code: intact DNA (Form I, green block), single-strand scission (Form II, yellow block), and double-strand scission (Form III, red block).

enediyne molecules in the minor groove of DNA[62] and cutting both strands of DNA in a single event. Meanwhile, the possibility that multiple binding/cleavage events take place with more than one drug molecules involved should not be ruled out either.[65] To differentiate the direct ds cleavage from the random path due to multiple ss breaks, further statistical analysis was conducted using the Poisson distribution $f(\mathrm{III}) = n2 \exp(-n2)$ and the Freifelder−Trumbo equation[66,67] $f(\mathrm{I}) = \exp[-(n1 + n2)]$. According to the fraction of supercoiled $f(\mathrm{I})$ and linear $f(\mathrm{III})$ DNA from each experiment, the average numbers of single-strand breaks ($n1$) and double-strand breaks ($n2$) per DNA molecule were calculated from the above equations. The $n1/n2$ ratio shown in Table S2 (ranging from 0.1 to 6.3) is much lower than 100, which clearly indicated that both enediynes caused ds cleavage through a concerted mechanism rather than the random pattern. This surprising finding is distinct from many kinds of small molecular enediyne compounds, suggesting the high possibility of the placement of these enediynes in the minor groove of DNA. The mechanism

https://dx.doi.org/10.1021/acs.joc.0c01124
J. Org. Chem. 2020, 85, 9808−9819

of this intriguing binding is still under investigation. Nevertheless, the efficient DNA cleavage and especially high percentage of ds DNA cleavage of both enediynes at millimolar concentration in physiologically relevant environments endows their high cytotoxicity toward tumor cells.

Cytotoxicity Assays. The ability of enediynes to induce cell death was evaluated by the 3-(4,5-dimethyl-2-thiazolyl)-2,5-diphenyl-2-*H*-tetrazolium bromide (MTT) assay (Figure S5). Three kinds of cancer cell lines, human cervical cancer (Hela), human breast adenocarcinoma (MCF-7), and human liver carcinoma (HepG2), were used for these experiments. The half-maximum inhibition concentrations (IC_{50}) of the enediynes toward cancer cells are listed in Table 1. The

Table 1. In Vitro Cytotoxicity of Enediynes against Three Kinds of Tumor Cell Lines and Their Physicochemical Data

	IC_{50} (μM)			physicochemical properties		
compound	Hela	MCF-7	HepG2	log*P*	tPSA (Å^2)	MW (Da)
EDY-A	>50	>50	>50	5.7	59.1	496
EDY-B	5.8	7.3	8.2	3.2	122.8	629
EDY-C	1.6	2.5	2.1	1.6	113.4	502
EDY-D	0.96	1.4	1.2	3.4	93.2	500
EDY-E	2.3	3.0	3.0	1.4	113.4	488
EDY-F	0.54	1.2	1.1	0.9	83.9	331

extremely high IC_{50} values of **EDY-A** indicate its low toxicity due to its incapability to generate radical species in physiological environments. On the other hand, taking advantage of the MARACA mechanism, all of the maleimide-based enediynes exhibit significant cytotoxicity toward all three kinds of cancer cells. The IC_{50} values range from micromolar to submicromolar levels, comparable to or even higher than many commercial antitumor agents like cisplatin[68,69] and doxorubicin.[70] As essential properties for small molecular drugs, solubility and permeability are measured by log*P* and topological polar surface area (tPSA) values.[71] The differences in potency among maleimide-enediynes are the result of a substituent effect to modulate relevant physicochemical properties as stated by Lipinski's rule of five (Ro5)[72] for drug-likeness criteria.

Cellular Uptake. Based on the considerably high thermal reactivity of enediynes in polar solvent and the unique free-radical-involved direct DNA interaction/damage mechanism, the efficiency of enediynes entering the cells or even the cell nucleus is crucial to their cytotoxicity performance. By taking advantage of the inherent fluorescent property of these maleimide-based enediynes (Figure S6), their cellular uptake was directly visualized by confocal laser scanning microscopy (CLSM). Figure 7A shows that **EDY-F** mainly enriches in cell nuclei, whereas **EDY-B** enriches in cell cytoplasm for the most of HeLa cells after 4−8 h incubation. The difference in cellular accumulation locations might be responsible for the distinct efficacy of cytotoxicity, as observed from **EDY-B** and **EDY-F** (Table 1).

Intracellular DNA Damage Assay. Given the DNA-targeted cytotoxic mechanism of enediynes, the intracellular enediyne-induced DNA-damaging activity was investigated using γ-H2AX foci analysis. γ-H2AX is a DNA double-strand break (DSB) marker that can create γ-H2AX foci at or near the

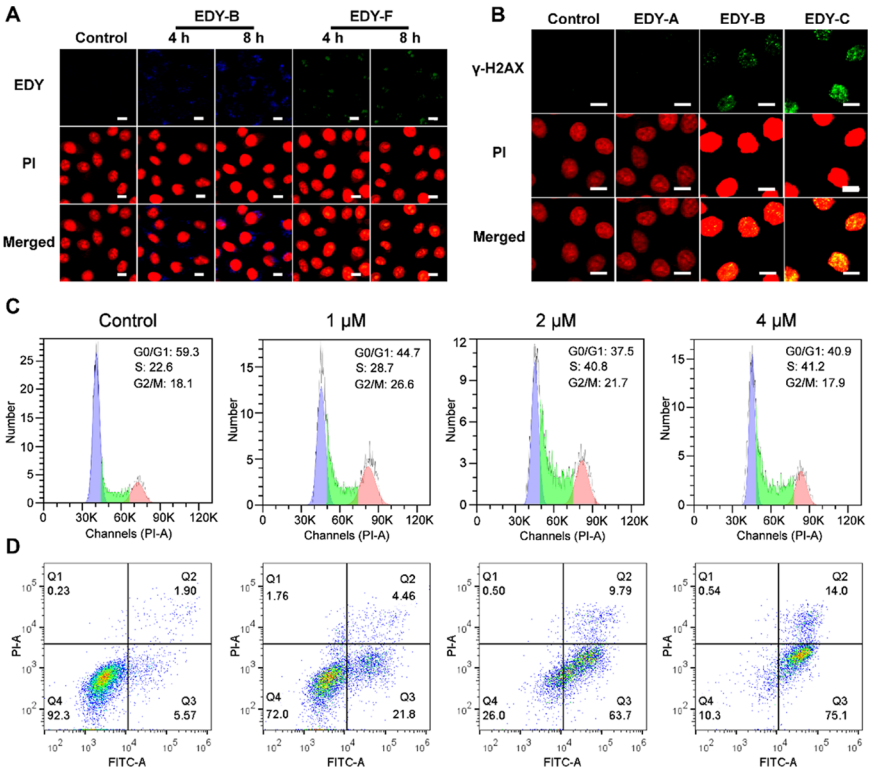

Figure 7. (A) Cellular uptake CLSM analysis of Hela cells treated with **EDY-B** (6 μM) or **EDY-F** (1 μM) after 4 or 8 h incubation. Cell nuclei are stained with PI (red). The scale bar is 10 μm. (B) γ-H2AX foci immunofluorescence staining of Hela cells treated with **EDY-A** (6 μM), **EDY-B** (6 μM), or **EDY-C** (2 μM). Cell nuclei are stained with PI (red). The scale bar is 10 μm. (C) Cell cycle distribution of Hela cells treated with **EDY-F** of varied concentrations for 24 h and then analyzed by flow cytometry. (D) Cell apoptosis assay of Hela cells treated with **EDY-F** of varied concentrations for 24 h and then analyzed by flow cytometry.

https://dx.doi.org/10.1021/acs.joc.0c01124
J. Org. Chem. 2020, 85, 9808−9819

DNA damage site and can be visualized by immunofluorescence.[73] Comparing with the negligible γ-H2AX foci formation in the **EDY-A** sample, the green fluorescent spots of γ-H2AX foci in **EDY-B** and **EDY-C** are obvious (Figure 7B), indicating the generated diradicals via MARACA, which resulted in DNA-damaging activity in living cells. Combining with the extracellular DNA cleavage study above, these results corroborate the ds DNA break effect stemming from maleimide-based enediynes.

Cell Cycle Arrest and Apoptosis Assay. Intracellular DNA damage resulting from environmental toxicants may activate cell cycle checkpoint arrest and induce cell apoptosis.[74] Encouraged by cell viability inhibition of **EDY-F** with an IC_{50} value of 0.54 μM against Hela cells, **EDY-F** was used to examine the cell cycle arrest ability and to investigate the cell death pathway of Hela cells. To this end, Hela cells were treated with **EDY-F** in different concentrations (1, 2, and 4 μM, respectively) for 24 h. The cell cycle distribution was determined by flow cytometry, as shown in Figure 7C. **EDY-F** arrests the cell cycle at the S phase in a dose-dependent manner, which reveals that the **EDY-F** may display its cytotoxicity through the inhibition of DNA replication process[75] and that the generated diradicals greatly contribute to this effect via direct DNA interaction and damage. To further evaluate the cell death pathways induced by **EDY-F**, Annexin V-FITC/PI staining assay is carried out. Hela cells were treated with **EDY-F** of 1, 2, and 4 μM, respectively. The fractions of viable, early apoptotic, late apoptotic, and necrotic cells were quantified by flow cytometry. Figure 7D shows that **EDY-F** causes cell apoptosis at the concentration of 1 μM (*Q*2 + *Q*3 = 26%), and significant apoptosis behavior is observed at 4 μM (*Q*2 + *Q*3 = 89%). All of these results confirm that the diradicals generated through the MARACA mechanism lead to effective S phase block and promote apoptotic response, eventually triggering the antitumor potency of acyclic enediynes.

CONCLUSIONS

In summary, we have uncovered a new mechanism named as MARACA to trigger the antitumor potency of acyclic enediynes. The presence of maleimide moiety was proved to be essential for the cascade 1,3-proton shift processes and for transforming the otherwise nonreactive acyclic enediynes to reactive enyne-allenes in physiologically relevant environments. The first-order kinetics of the enediyne compounds suggest the intramolecular cycloaromatization (MSC) being the rate-limiting step in the MARACA mechanism, which was further confirmed with theoretical computation. The distinct effect of solvent polarity on the overall reactivity of these enediyne compounds endows them with capability for further derivatization, long-term storage, and drug delivery without compromising their high reactivity in polar media. The generated free radicals lead to high percentage of ds DNA damage and cytotoxicity to all tested cancer cell lines with IC_{50} values of micromolar to submicromolar level. Intracellular studies of enediynes indicated that the radical-involved DNA damage activity induced cell death via apoptosis mechanism. Overall, this MARACA mechanism provides a strategy to design simple yet robust acyclic enediyne antitumor agents for potential clinical applications.

EXPERIMENTAL SECTION

General Experimental Methods. Toluene, tetrahydrofuran (THF), and dichloromethane (DCM) were dried over calcium hydride (CaH_2) and distilled before use. 3-[4,5-Dimethylthiazol-2-yl]-2,5-diphenyltetrazolium-bromide (MTT) was obtained from Macklin. Annexin V-FITC/PI apoptosis detection kit, phospho-histone H2A.X (Ser139) rabbit monoclonal antibody, and Alexa Fluor 488-labeled Goat Anti-Rabbit IgG (H+L) were purchased from Beyotime Biotechnology. Dulbecco's modified Eagle's medium (DMEM), fetal bovine serum (FBS), and phosphate-buffered saline (PBS) were provided by BBI Life Sciences Corporation. Other reagents were purchased at commercial grade and used without further purification. Sonogashira reactions were performed with dry Schlenk techniques under an atmosphere of nitrogen.

^1H NMR and $^{13}C\{^1H\}$ NMR spectra were recorded on Bruker DRX-400, DRX-500, or DRX-600 instruments and calibrated using residual undeuterated solvent ($CDCl_3$: δ_H = 7.26 ppm, δ_C = 77.2 ppm; CD_3OD: δ_H = 3.31 ppm, δ_C = 49.0 ppm) as an internal reference. High-resolution mass spectra (HR-MS) were obtained on a Micromass LCTTM mass spectrometer using the ESI or EI method. The electron paramagnetic resonance (EPR) measurements were performed with an X-band EMX-8/2.7C EPR spectrometer (Bruker). Fluorescence spectra were recorded on a PerkinElmer LS-55 (excited at 350 nm). Absorbance spectra were collected using a UV−vis spectrophotometer (Lambda Bio40, PerkinElmer). Differential scanning calorimetry (DSC) was carried out with a Pyris Diamond thermal analysis workstation equipped with a model 822e DSC module under a constant nitrogen flow. Cytotoxicity assay was measured by a microplate reader (Thermo Scientific). Fluorescence microscopy images were taken using a confocal laser scanning microscope (CLSM, Nikon). Quantitative flow cytometry was recorded by a flow cytometer (Beckman).

***N*-(*tert*-Butyl)prop-2-yn-1-amine (1s).**[40] To a stirred solution of 2-methylpropan-2-amine (52.5 mL, 500 mmol) in DCM (100 mL), 3-bromo-1-propyne (8.6 mL, 100 mmol) was added dropwise at room temperature. After stirring for 36 h, the reaction mixture was washed three times with water. The resulting organic phase was dried over $MgSO_4$, filtered, and the solvent was evaporated under reduced pressure. The product was purified by distillation to give a pale yellow oil (8.8 g, 79%). All spectroscopic data were in accordance with the literature.

***tert*-Butyl *tert*-Butyl(prop-2-yn-1-yl)carbamate (1).** *N*-(*tert*-Butyl)prop-2-yn-1-amine (**1s**, 4.0 g, 36 mmol) was dissolved in DCM (40 mL) with subsequent addition of $(Boc)_2O$ (12.4 mL, 54 mmol). The mixture was stirred at reflux in an oil bath for 36 h, then cooled to room temperature. Imidazole (6.0 g, 36 mmol) was added to consume the excess $(Boc)_2O$ completely.[76] After removal of the solvent under vacuum, the crude residue was partitioned between ethyl acetate (50 mL) and 1% HCl (50 mL). The resulting organic phase was washed with 1% HCl (2 × 50 mL) and brine (2 × 50 mL), dried over $MgSO_4$, filtered, and concentrated. The crude product was purified by column chromatography on silica gel (hexane/ethyl acetate = 50:1) to give compound **1** as a pale yellow oil (6.4 g, 84%); ^1H NMR (500 MHz, $CDCl_3$) δ 4.05 (d, *J* = 2.1 Hz, 2H), 2.13 (t, *J* = 2.2 Hz, 1H), 1.45 (s, 9H), 1.42 (s, 9H); $^{13}C\{^1H\}$ NMR (126 MHz, $CDCl_3$) δ 155.2, 82.2, 79.9, 70.2, 55.9, 34.1, 29.2, 28.4; HRMS (ESI-TOF) *m*/*z*: $[M + Na]^+$ calcd for $C_{12}H_{21}NO_2Na$ 234.1470; found 234.1471.

***tert*-Butyl 2-(3,4-Dichloro-2,5-dioxo-2,5-dihydro-1*H*-pyrrol-1-yl)acetate (2s).**[41] Glycine tert butyl ester hydrochloride (11.0 g, 66 mmol) was added to a solution of dichloromaleic anhydride (12.0 g, 72 mmol) and potassium acetate (6.5 g, 66 mmol) in acetic acid (80 mL). The mixture was heated in an oil bath to 40 °C for 40 h. After removal of the solvent, the crude residue was partitioned between DCM (50 mL) and H_2O (50 mL). The resulting organic phase was washed with H_2O (2 × 50 mL), dried over $MgSO_4$, filtered, and concentrated. The crude product was separated by column chromatography on silica gel (hexane/ethyl acetate = 10:1) to give

https://dx.doi.org/10.1021/acs.joc.0c01124
J. Org. Chem. 2020, 85, 9808−9819

the product as a white solid (11.5 g, 62%). All spectroscopic data were in accordance with the literature.

***tert*-Butyl 2-(3,4-Diiodo-2,5-dioxo-2,5-dihydro-1*H*-pyrrol-1-yl)acetate (2).**[41] A solution of sodium iodide (15.0 g, 100 mmol) and *tert*-butyl 2-(3,4-dichloro-2,5-dioxo-2,5-dihydro-1*H*-pyrrol-1-yl)-acetate (**2s**, 7.0 g, 25 mmol) in acetonitrile (50 mL) was heated at reflux in an oil bath for 12 h. Then, the mixture was concentrated under reduced pressure. The crude product was purified by column chromatography on silica gel (hexane/ethyl acetate = 10:1) to afford a pale yellow solid (10.6 g, 92%). All spectroscopic data were in accordance with the literature.

3,4-Dichloro-1-neopentyl-1*H*-pyrrole-2,5-dione (3s). Dichloromaleic anhydride (6.7 g, 40 mmol) was dissolved in acetic acid (70 mL) with slow addition of neopentylamine (3.2 g, 36 mmol). The mixture was then heated at reflux in an oil bath for 8 h. After removal of the solvent, the resulting crude residue was separated by column chromatography on silica gel (hexane/ethyl acetate = 10:1) to give the product as a yellow solid (7.0 g, 83%); ^{1}H NMR (400 MHz, CD_3OD) δ 3.37 (s, 2H), 0.93 (s, 9H); $^{13}C\{^1H\}$ NMR (101 MHz, CD_3OD) δ 165.1, 134.1, 51.6, 34.2, 28.2; HRMS (EI) *m*/*z*: $[M]^+$ calcd for $C_9H_{11}Cl_2NO_2$ 235.0167; found 235.0170.

3,4-Diiodo-1-neopentyl-1*H*-pyrrole-2,5-dione (4s). A solution of sodium iodide (6.0 g, 40 mmol) and 3,4-dichloro-1-neopentyl-1*H*-pyrrole-2,5-dione (**3s**, 2.4 g, 10 mmol) in acetonitrile (50 mL) was stirred at reflux in an oil bath for 12 h. Then, the solution was concentrated under reduced pressure. The crude product was purified by column chromatography on silica gel (hexane/ethyl acetate = 10:1) to afford a yellow solid (3.4 g, 82%); ^{1}H NMR (400 MHz, $CDCl_3$) δ 3.40 (s, 2H), 0.90 (s, 9H); $^{13}C\{^1H\}$ NMR (101 MHz, $CDCl_3$) δ 167.1, 117.5, 51.6, 33.7, 28.0; HRMS (EI) *m*/*z*: $[M]^+$ calcd for $C_9H_{11}I_2NO_2$ 418.8879; found 418.8884.

Di-*tert*-butyl (1,2-Phenylenebis(prop-2-yne-3,1-diyl))bis-(*tert*-butylcarbamate) (EDY-A). 1,2-Diiodobenzene (165.0 mg, 0.5 mmol), CuI (38.1 mg, 40%), $(PPh_3)_2PdCl_2$ (35.1 mg, 10%), and *n*-$BuNH_2$ (109.7 mg, 1.5 mmol) were successively added to dry THF (4 mL) solution under nitrogen. Then, compound **1** (316.5 mg, 1.5 mmol) in THF (1 mL) was added dropwise. The mixture was stirred at ambient temperature for 18 h. After the completion of the reaction, as detected by TLC, the mixture was directly purified by column chromatography on silica gel (hexane/ethyl acetate = 20:1) to yield a yellow oil (136 mg, 55%); ^{1}H NMR (600 MHz, $CDCl_3$) δ 7.38 (dd, *J* = 5.7, 3.4 Hz, 2H), 7.21 (dd, *J* = 5.8, 3.3 Hz, 2H), 4.34 (s, 4H), 1.51 (s, 18H), 1.49 (s, 18H); $^{13}C\{^1H\}$ NMR (151 MHz, $CDCl_3$) δ 155.5, 132.3, 127.8, 125.6, 91.5, 81.2, 80.1, 56.1, 35.3, 29.5, 28.7; HRMS (ESI-TOF) *m*/*z*: $[M + Na]^+$ calcd for $C_{30}H_{44}N_2O_4Na$ 519.3199; found 519.3198.

***tert*-Butyl 2-(3,4-bis(3-((*tert*-butoxycarbonyl)(*tert*-butyl)-amino)prop-1-yn-1-yl)-2,5-dioxo-2,5-dihydro-1*H*-pyrrol-1-yl)-acetate (EDY-B).** Compound **2** (231.4 mg, 0.5 mmol), CuI (38.1 mg, 40%), $(PPh_3)_2PdCl_2$ (35.1 mg, 10%), and DIPEA (193.9 mg, 1.5 mmol) were successively added to a solvent mixture of dry THF (3 mL) and toluene (6 mL) under nitrogen. Then, compound **1** (316.6 mg, 1.5 mmol) in THF (1 mL) was added dropwise. The mixture was stirred at ambient temperature for 12 h. After the completion of the reaction, as detected by TLC, the mixture was directly purified by column chromatography on silica gel (hexane/ethyl acetate = 10:1) to yield a yellow oil (32 mg, 10%); ^{1}H NMR (500 MHz, $CDCl_3$) δ 4.40 (s, 4H), 4.14 (s, 2H), 1.47 (s, 18H), 1.46 (s, 18H), 1.43 (s, 9H); $^{13}C\{^1H\}$ NMR (126 MHz, $CDCl_3$) δ 166.4, 166.0, 155.2, 128.3, 109.1, 83.2, 80.6, 73.1, 56.4, 40.3, 35.6, 29.5, 28.6, 28.1; HRMS (ESI-TOF) *m*/*z*: $[M + Na]^+$ calcd for $C_{34}H_{51}N_3O_8Na$ 652.3574; found 652.3573.

***tert*-Butyl 2-(4-(2-((*tert*-butoxycarbonyl)(*tert*-butyl)amino)-ethyl)-3-(*tert*-butyl)-2,5,7-trioxo-2,3,5,7-tetrahydro-6*H*-oxazolo[4,5-*f*]isoindol-6-yl)acetate (compound 3).** Isolated as a yellow solid (35 mg, 12%) from the synthesis procedure of EDY-B; ^{1}H NMR (500 MHz, $CDCl_3$) δ 7.45 (s, 1H), 4.29 (s, 2H), 3.59 (t, *J* = 6.5 Hz, 2H), 3.45 (t, *J* = 6.5 Hz, 2H), 1.74 (s, 9H), 1.45 (s, 9H), 1.37 (s, 9H), 1.31 (s, 9H); $^{13}C\{^1H\}$ NMR (126 MHz, $CDCl_3$) δ 168.1, 166.6, 166.4, 156.0, 153.4, 147.7, 136.0, 128.4, 127.1, 126.0, 103.3, 83.0, 80.0, 60.6, 55.8, 46.3, 39.9, 34.1, 30.2, 30.0, 28.6, 28.1; HRMS (ESI-TOF) *m*/*z*: $[M + Na]^+$ calcd for $C_{30}H_{43}N_3O_8Na$ 596.2948; found 596.2949.

General Procedure for the Synthesis of EDY-C, D, and E. Compound **2** (231.4 mg, 0.5 mmol), CuI (38.1 mg, 40%), $(PPh_3)_2PdCl_2$ (35.1 mg, 10%), and DIPEA (193.9 mg, 1.5 mmol) were successively added to a solvent mixture of dry THF (2 mL) and toluene (4 mL) under nitrogen. Then, compound **1** (158.3 mg, 0.75 mmol) and the corresponding another terminal alkyne (0.75 mmol, commercially available) in THF (1 mL) were added dropwise. The mixture was stirred at ambient temperature overnight. After the completion of the reaction, as detected by TLC, the mixture was directly purified by column chromatography on silica gel (eluted with 75−90% hexane/ethyl acetate) to give the product.

***tert*-Butyl 2-(3-(3-((*tert*-butoxycarbonyl)(*tert*-butyl)amino)-prop-1-yn-1-yl)-4-(3-hydroxy-3 methylbut-1-yn-1-yl)-2,5-dioxo-2,5-dihydro-1*H*-pyrrol-1-yl)acetate (EDY-C).** Pale yellow oil, 18% (45 mg); ^{1}H NMR (600 MHz, $CDCl_3$) δ 4.44 (s, 2H), 4.17 (s, 2H), 1.60 (s, 6H), 1.49 (s, 9H), 1.49 (s, 9H), 1.45 (s, 9H); $^{13}C\{^1H\}$ NMR (151 MHz, $CDCl_3$) δ 166.5, 166.4, 165.9, 155.4, 128.9, 128.5, 114.4, 109.7, 83.2, 80.8, 73.0, 72.5, 65.9, 56.5, 40.4, 35.8, 31.0, 29.7, 28.7, 28.1; HRMS (ESI-TOF) *m*/*z*: $[M + Na]^+$ calcd for $C_{27}H_{38}N_2O_7Na$ 525.2577; found 525.2576.

***tert*-Butyl 2-(3-(3-((*tert*-butoxycarbonyl)(*tert*-butyl)amino)-prop-1-yn-1-yl)-4-(3,3-dimethylbut-1-yn-1-yl)-2,5-dioxo-2,5-dihydro-1*H*-pyrrol-1-yl)acetate (EDY-D).** Pale yellow oil, 26% (65 mg); ^{1}H NMR (600 MHz, $CDCl_3$) δ 4.43 (s, 2H), 4.15 (s, 2H), 1.49 (s, 9H), 1.48 (s, 9H), 1.44 (s, 9H), 1.32 (s, 9H); $^{13}C\{^1H\}$ NMR (151 MHz, $CDCl_3$) δ 166.9, 166.7, 166.0, 155.2, 129.4, 127.4, 120.6, 108.2, 83.1, 80.5, 73.1, 70.4, 56.4, 40.3, 35.7, 30.5, 29.6, 29.2, 28.6, 28.1; HRMS (ESI-TOF) *m*/*z*: $[M + Na]^+$ calcd for $C_{28}H_{40}N_2O_6Na$ 523.2784; found 523.2783.

***tert*-Butyl 2-(3-(3-((*tert*-butoxycarbonyl)(*tert*-butyl)amino)-prop-1-yn-1-yl)-4-(4-hydroxybut-1-yn-1-yl)-2,5-dioxo-2,5-dihydro-1*H*-pyrrol-1-yl)acetate (EDY-E).** Pale yellow oil, 20% (49 mg); ^{1}H NMR (600 MHz, $CDCl_3$) δ 4.42 (s, 2H), 4.16 (s, 2H), 3.83 (t, *J* = 6.2 Hz, 2H), 2.79 (t, *J* = 6.2 Hz, 2H), 1.49 (s, 9H), 1.48 (s, 9H), 1.44 (s, 9H); $^{13}C\{^1H\}$ NMR (151 MHz, $CDCl_3$) δ 166.8, 166.6, 165.9, 155.4, 129.3, 128.5, 109.4, 109.1, 83.2, 80.7, 73.1, 72.9, 60.5, 56.5, 40.4, 35.8, 29.6, 28.6, 28.1, 25.0; HRMS (ESI-TOF) *m*/*z*: $[M + Na]^+$ calcd for $C_{26}H_{36}N_2O_7Na$ 511.2420; found 511.2421.

3-(4-(4-Hydroxybut-1-yn-1-yl)-1-neopentyl-2,5-dioxo-2,5-dihydro-1*H*-pyrrol-3-yl)prop-2-yn-1-yl Acetate (EDY-F). Compound **10** (209.4 mg, 0.5 mmol), CuI (38.1 mg, 40%), $(PPh_3)_2PdCl_2$ (35.1 mg, 10%), and DIPEA (193.9 mg, 1.5 mmol) were successively added to a solvent mixture of dry THF (2 mL) and toluene (4 mL) under nitrogen. Then, prop-2-yn-1-yl acetate (73.5 mg, 0.75 mmol) and but-3-yn-1-ol (52.5 mg, 0.75 mmol) in THF (1 mL) were added dropwise. The mixture was stirred at ambient temperature overnight. After the completion of the reaction, as detected by TLC, the mixture was directly purified by column chromatography on silica gel (hexane/ethyl acetate = 2:1) to give the product as a pale yellow oil, 26% (43 mg); ^{1}H NMR (600 MHz, $CDCl_3$) δ 4.95 (s, 2H), 3.85 (t, *J* = 6.3 Hz, 2H), 3.33 (s, 2H), 2.83 (t, *J* = 6.3 Hz, 2H), 2.12 (s, 3H), 0.89 (s, 9H); $^{13}C\{^1H\}$ NMR (151 MHz, $CDCl_3$) δ 170.3, 167.6, 130.4, 127.0, 110.5, 102.2, 76.2, 73.0, 60.4, 52.6, 50.3, 33.7, 28.0, 25.1, 20.8; HRMS (ESI-TOF) *m*/*z*: $[M + Na]^+$ calcd for $C_{18}H_{21}NO_5Na$ 354.1317; found 354.1316.

■ ASSOCIATED CONTENT

Supporting Information

The Supporting Information is available free of charge at https://pubs.acs.org/doi/10.1021/acs.joc.0c01124.

Experimental procedure and fundamental characterization (PDF)

data_mjr18069 (CIF)

https://dx.doi.org/10.1021/acs.joc.0c01124
J. Org. Chem. 2020, 85, 9808−9819

AUTHOR INFORMATION

Corresponding Authors

Yun Ding − *Shanghai Key Laboratory of Advanced Polymeric Materials, School of Materials Science and Engineering, East China University of Science and Technology, Shanghai 200237, China*; Email: yunding@ecust.edu.cn

Aiguo Hu − *Shanghai Key Laboratory of Advanced Polymeric Materials, School of Materials Science and Engineering, East China University of Science and Technology, Shanghai 200237, China*; orcid.org/0000-0003-0456-7269; Email: hagmhsn@ecust.edu.cn

Authors

Mengsi Zhang − *Shanghai Key Laboratory of Advanced Polymeric Materials, School of Materials Science and Engineering, East China University of Science and Technology, Shanghai 200237, China*

Baojun Li − *Shanghai Key Laboratory of Advanced Polymeric Materials, School of Materials Science and Engineering, East China University of Science and Technology, Shanghai 200237, China*

Huimin Chen − *Shanghai Key Laboratory of Advanced Polymeric Materials, School of Materials Science and Engineering, East China University of Science and Technology, Shanghai 200237, China*

Haotian Lu − *Shanghai Key Laboratory of Advanced Polymeric Materials, School of Materials Science and Engineering, East China University of Science and Technology, Shanghai 200237, China*

Hailong Ma − *Shanghai Key Laboratory of Advanced Polymeric Materials, School of Materials Science and Engineering, East China University of Science and Technology, Shanghai 200237, China*

Xiaoyu Cheng − *Shanghai Key Laboratory of Advanced Polymeric Materials, School of Materials Science and Engineering, East China University of Science and Technology, Shanghai 200237, China*

Wenbo Wang − *Shanghai Key Laboratory of Advanced Polymeric Materials, School of Materials Science and Engineering, East China University of Science and Technology, Shanghai 200237, China*

Yue Wang − *Shanghai Key Laboratory of Advanced Polymeric Materials, School of Materials Science and Engineering, East China University of Science and Technology, Shanghai 200237, China*

Complete contact information is available at: https://pubs.acs.org/10.1021/acs.joc.0c01124

Author Contributions

The manuscript was written through contributions of all authors.

Notes

The authors declare no competing financial interest.

ACKNOWLEDGMENTS

The authors gratefully acknowledge the financial support from National Natural Science Foundation of China (21871080, 21503078), the Fundamental Research Funds for the Central Universities (22221818014), and Shanghai Leading Academic Discipline Project (B502). A.H. thanks the "Eastern Scholar Professorship" support from Shanghai local government. A.H. thanks Profs. Runhui Liu and Junyou Wang for their kind help in cellular experiments.

REFERENCES

(1) Chang, C.-Y.; Yan, X.; Crnovcic, I.; Annaval, T.; Chang, C.; Nocek, B.; Rudolf, J. D.; Yang, D.; Hindra; Babnigg, G.; Joachimiak, A.; Phillips, G. N.; Shen, B. Resistance to Enediyne Antitumor Antibiotics by Sequestration. *Cell Chem. Biol.* **2018**, *25*, 1075−1085.

(2) Nicolaou, K. C.; Dai, W. M. Chemistry and Biology of the Enediyne Anticancer Antibiotics. *Angew. Chem., Int. Ed.* **1991**, *30*, 1387−1416.

(3) DiJoseph, J. F.; Dougher, M. M.; Armellino, D. C.; Kalyandrug, L.; Kunz, A.; Boghaert, E. R.; Hamann, P. R.; Damle, N. K. CD20-specific antibody-targeted chemotherapy of non-Hodgkin's B-cell lymphoma using calicheamicin-conjugated rituximab. *Cancer Immunol. Immunother.* **2007**, *56*, 1107−1117.

(4) DiJoseph, J. F.; Armellino, D. C.; Boghaert, E. R.; Khandke, K.; Dougher, M. M.; Sridharan, L.; Kunz, A.; Hamann, P. R.; Gorovits, B.; Udata, C.; Moran, J. K.; Popplewell, A. G.; Stephens, S.; Frost, P.; Damle, N. K. Antibody-targeted chemotherapy with CMC-544: a CD22-targeted immunoconjugate of calicheamicin for the treatment of B-lymphoid malignancies. *Blood* **2004**, *103*, 1807−1814.

(5) Hamann, P. R.; Hinman, L. M.; Beyer, C. F.; Lindh, D.; Upeslacis, J.; Flowers, D. A.; Bernstein, I. An Anti-CD33 Antibody-Calicheamicin Conjugate for Treatment of Acute Myeloid Leukemia. Choice of Linker. *Bioconjugate Chem.* **2002**, *13*, 40−46.

(6) Sapra, P.; Shor, B. Monoclonal antibody-based therapies in cancer: Advances and challenges. *Pharmacol. Ther.* **2013**, *138*, 452−469.

(7) Siegel, R.; Ma, J.; Zou, Z.; Jemal, A. Cancer statistics, 2014. *CA Cancer J. Clin.* **2014**, *64*, 9−29.

(8) Torre, L. A.; Bray, F.; Siegel, R. L.; Ferlay, J.; Lortet-Tieulent, J.; Jemal, A. Global cancer statistics, 2012. *CA Cancer J. Clin.* **2015**, *65*, 87−108.

(9) Cao, Y.; DePinho, R. A.; Ernst, M.; Vousden, K. Cancer research: past, present and future. *Nat. Rev. Cancer* **2011**, *11*, 749−754.

(10) Cragg, G. M.; Kingston, D. G.; Newman, D. J. *Anticancer Agents from Natural Products*; CRC Press, 2011.

(11) Porter, M. R.; Lindahl, S. E.; Lietzke, A.; Metzger, E. M.; Wang, Q.; Henck, E.; Chen, C.-H.; Niu, H.; Zaleski, J. M. Metal-mediated diradical tuning for DNA replication arrest via template strand scission. *Proc. Natl. Acad. Sci. U.S.A.* **2017**, *114*, E7405−E7414.

(12) Baker, J. R.; Woolfson, D. N.; Muskett, F. W.; Stoneman, R. G.; Urbaniak, M. D.; Caddick, S. Protein−Small Molecule Interactions in Neocarzinostatin, the Prototypical Enediyne Chromoprotein Antibiotic. *ChemBioChem* **2007**, *8*, 704−717.

(13) Jones, G. B.; Plourde, G. W.; Wright, J. M. Understanding Enediyne-Protein Interactions: Diyl Atom Transfer Results in Generation of Aminoacyl Radicals. *Org. Lett.* **2000**, *2*, 811−813.

(14) Kawata, S.; Ashizawa, S.; Hirama, M. Synthetic Study of Kedarcidin Chromophore: Revised Structure. *J. Am. Chem. Soc.* **1997**, *119*, 12012−12013.

(15) Dedon, P. C.; Jiang, Z. W.; Goldberg, I. H. Neocarzinostatin-mediated DNA damage in a model AGT.cntdot.ACT site: mechanistic studies of thiol-sensitive partitioning of C4′ DNA damage products. *Biochemistry* **1992**, *31*, 1917−1927.

(16) Kappen, L.; Goldberg, I. DNA conformation-induced activation of an enediyne for site-specific cleavage. *Science* **1993**, *261*, 1319−1321.

(17) Ishida, N.; Miyazaki, K.; Kumagai, K.; Rikimaru, M. Neocarzinostatin, antitumor antibiotic of high molecular weight; isolation, physicochemical properties, and biological activities. *J. Antibiot., Ser. A* **1965**, *18*, 68−76.

(18) Koga, N.; Morokuma, K. Comparison of biradical formation between enediyne and enyne-allene. Ab initio CASSCF and MRSDCI study. *J. Am. Chem. Soc.* **1991**, *113*, 1907−1911.

(19) Alabugin, I. V.; Manoharan, M. Reactant Destabilization in the Bergman Cyclization and Rational Design of Light- and pH-Activated Enediynes. *J. Phys. Chem. A* **2003**, *107*, 3363−3371.
(20) dos Passos Gomes, G.; Alabugin, I. V. Drawing Catalytic Power from Charge Separation: Stereoelectronic and Zwitterionic Assistance in the Au(I)-Catalyzed Bergman Cyclization. *J. Am. Chem. Soc.* **2017**, *139*, 3406−3416.
(21) Mohamed, R. K.; Peterson, P. W.; Alabugin, I. V. Concerted Reactions That Produce Diradicals and Zwitterions: Electronic, Steric, Conformational, and Kinetic Control of Cycloaromatization Processes. *Chem. Rev.* **2013**, *113*, 7089−7129.
(22) Kar, M.; Basak, A. Design, Synthesis, and Biological Activity of Unnatural Enediynes and Related Analogues Equipped with pH-Dependent or Phototriggering Devices. *Chem. Rev.* **2007**, *107*, 2861−2890.
(23) Cunico, R. F.; Nair, S. K. Cycloaromatization of a solvolytically generated ene-yne-allene. *Tetrahedron Lett.* **1997**, *38*, 25−28.
(24) Ferri, F.; Brückner, R.; Herges, R. Straightforward syntheses of biradical-producing bicyclic dienediynes-dienediyne ketones cycloaromatize ia the Saito-Myers and not ia the neocarzinostatin pathway. *New J. Chem.* **1998**, *22*, 531−546.
(25) Li, Y.; Kirillov, A. M.; Fang, R.; Yang, L. Effect of Substituent on the Mechanism and Chemoselectivity of the Gold(I)-Catalyzed Propargyl Ester Tandem Cyclization. *Organometallics* **2017**, *36*, 1164−1172.
(26) Raviola, C.; Protti, S.; Ravelli, D.; Fagnoni, M. (Hetero)-aromatics from dienynes, enediynes and enyne-allenes. *Chem. Soc. Rev.* **2016**, *45*, 4364−4390.
(27) Grissom, J. W.; Huang, D. Tandem Eneyne Allene-Radical Cyclization via [3,3] Sigmatropic Rearrangements. *J. Org. Chem.* **1994**, *59*, 5114−5116.
(28) Sun, S.; Zhu, C.; Song, D.; Li, F.; Hu, A. Preparation of Conjugated Polyphenylenes from Maleimide-Based Enediynes Through Thermal-Triggered Bergman Cyclization Polymerization. *Polym. Chem.* **2014**, *5*, 1241−1247.
(29) Li, J.; Li, B.; Sun, L.; Duan, B.; Huang, S.; Yuan, Y.; Ding, Y.; Hu, A. Self-delivery nanoparticles of an amphiphilic irinotecan−enediyne conjugate for cancer combination chemotherapy. *J. Mater. Chem. B* **2019**, *7*, 103−111.
(30) Li, B.; Duan, B.; Li, J.; Zhang, M.; Yuan, Y.; Ding, Y.; Hu, A. An Acyclic Enediyne Anticancer Compound Attributed to a Bergman Cyclization at Physiological Temperature. *Tetrahedron* **2018**, *74*, 6419−6425.
(31) Song, D.; Sun, S.; Tian, Y.; Huang, S.; Ding, Y.; Yuan, Y.; Hu, A. Maleimide-Based Acyclic Enediyne for Efficient DNA-Cleavage and Tumor Cell Suppression. *J. Mater. Chem. B* **2015**, *3*, 3195−3200.
(32) Lu, H.; Ma, H.; Li, B.; Zhang, M.; Chen, H.; Wang, Y.; Li, X.; Ding, Y.; Hu, A. Facilitating Myers-Saito cyclization through acid-triggered tautomerization for the development of maleimide-based antitumor agents. *J. Mater. Chem. B* **2020**, *8*, 1971−1979.
(33) Li, J.; Zhang, M.; Huang, S.; Ding, Y.; Hu, A. Concurrent Radical Addition and [3+2] Cycloaddition between Nitrones and Maleimide-Based Acyclic Enediynes. *Asian J. Org. Chem.* **2018**, *7*, 2076−2081.
(34) Das, E.; Basak, S.; Anoop, A.; Chand, S.; Basak, A. How To Achieve High Regioselectivity in Barrier-less Nucleophilic Addition to p-Benzynes Generated via Bergman Cyclization of Unsymmetrical Cyclic Azaenediyne? *J. Org. Chem.* **2019**, *84*, 2911−2921.
(35) Borie, C.; Mondal, S.; Arif, T.; Briand, M.; Lingua, H.; Dumur, F.; Gigmes, D.; Stocker, P.; Barbarat, B.; Robert, V.; Nicoletti, C.; Olive, D.; Maresca, M.; Nechab, M. Enediynes bearing polyfluoroaryl sulfoxide as new antiproliferative agents with dual targeting of microtubules and DNA. *Eur. J. Med. Chem.* **2018**, *148*, 306−313.
(36) Valenzuela, S. A.; Cortés, A. J.; Tippins, Z. J. E.; Daly, M. H.; Keel, T. E.; Gherman, B. F.; Spence, J. D. Effect of Extended Benzannelation Orientation on Bergman and Related Cyclizations of Isomeric Quinoxalenediynes. *J. Org. Chem.* **2017**, *82*, 13297−13312.
(37) Das, J.; Roy, S.; Halnor, S.; Das, A. K.; Basak, A. Enediyne-based protein capture agents: demonstration of an enediyne moiety acting as a photoaffinity label. *Org. Biomol. Chem.* **2017**, *15*, 1122−1129.
(38) Peterson, P. W.; Shevchenko, N.; Breiner, B.; Manoharan, M.; Lufti, F.; Delaune, J.; Kingsley, M.; Kovnir, K.; Alabugin, I. V. Orbital Crossings Activated through Electron Injection: Opening Communication between Orthogonal Orbitals in Anionic C1−C5 Cyclizations of Enediynes. *J. Am. Chem. Soc.* **2016**, *138*, 15617−15628.
(39) Campolo, D.; Arif, T.; Borie, C.; Mouysset, D.; Vanthuyne, N.; Naubron, J. V.; Bertrand, M. P.; Nechab, M. Double Transfer of Chirality in Organocopper-Mediated bis(Alkylating) Cycloisomerization of Enediynes. *Angew. Chem., Int. Ed.* **2014**, *53*, 3227−3231.
(40) Brunel, P.; Monot, J.; Kefalidis, C. E.; Maron, L.; Martin-Vaca, B.; Bourissou, D. Valorization of CO2: Preparation of 2-Oxazolidinones by Metal−Ligand Cooperative Catalysis with SCS Indenediide Pd Complexes. *ACS Catal.* **2017**, *7*, 2652−2660.
(41) Li, B.; Wu, Y.; Wang, Y.; Zhang, M.; Chen, H.; Li, J.; Liu, R.; Ding, Y.; Hu, A. Light-Cross-linked Enediyne Small-Molecule Micelle-Based Drug-Delivery System. *ACS Appl. Mater. Interfaces* **2019**, *11*, 8896−8903.
(42) Basak, A.; Kar, M. Benzofused N-substituted cyclic enediynes: Activation and DNA-cleavage potential. *Bioorg. Med. Chem.* **2008**, *16*, 4532−4537.
(43) Schmittel, M.; Maywald, M. Electronic effects in the thermal C2−C6 biradical cyclisation of enyne-allenes. *Chem. Commun.* **2001**, 155−156.
(44) Smith, D. W.; Shah, H. V.; Perera, K. P. U.; Perpall, M. W.; Babb, D. A.; Martin, S. J. Polyarylene networks via Bergman cyclopolymerization of bis-ortho-diynyl arenes. *Adv. Funct. Mater.* **2007**, *17*, 1237−1246.
(45) Roy, S.; Bag, S. S.; Basak, A. Synthesis and reactivity of enediyne−nucleobase hybrids: effect of intramolecular π-stacking. *Tetrahedron* **2012**, *68*, 8600−8611.
(46) Janzen, E. G.; Blackburn, B. J. Detection and identification of short-lived free radicals by an electron spin resonance trapping technique. *J. Am. Chem. Soc.* **1968**, *90*, 5909−5910.
(47) Iida, K.-i.; Hirama, M. Synthesis and Characterization of Nine-Membered Cyclic Enediynes, Models of the C-1027 and Kedarcidin Chromophores: Equilibration with a p-Benzyne Biradical and Kinetic Stabilization. *J. Am. Chem. Soc.* **1995**, *117*, 8875−8876.
(48) Zeidan, T. A.; Manoharan, M.; Alabugin, I. V. Ortho effect in the Bergman cyclization: Interception of p-benzyne intermediate by intramolecular hydrogen abstraction. *J. Org. Chem.* **2006**, *71*, 954−961.
(49) Usuki, T.; Nakanishi, K.; Ellestad, G. A. Spin-trapping of the p-benzyne intermediates from ten-membered enediyne calicheamicin gamma1I. *Org. Lett.* **2006**, *8*, 5461−5463.
(50) Usuki, T.; Kawai, M.; Nakanishi, K.; Ellestad, G. A. Calicheamicin gamma(I)(1) and phenyl tert-butyl nitrone (PBN): observation of a kinetic isotope effect by an ESR study. *Chem. Commun.* **2010**, *46*, 737−739.
(51) Hohenberg, P.; Kohn, W. Inhomogeneous Electron Gas. *Phys. Rev. B* **1964**, *136*, B864−B871.
(52) Kohn, W.; Sham, L. J. Self-Consistent Equations Including Exchange and Correlation Effects. *Phys. Rev.* **1965**, *140*, A1133−A1138.
(53) Frisch, M. J.; Trucks, G. W.; Schlegel, H. B.; Scuseria, G. E.; Robb, M. A.; Cheeseman, J. R.; Scalmani, G.; Barone, V.; Mennucci, B.; Petersson, G. A.; Nakatsuji, H.; Caricato, M.; Li, X.; Hratchian, H. P.; Izmaylov, A. F.; Bloino, J.; Zheng, G.; Sonnenberg, J. L.; Hada, M.; Ehara, M.; Toyota, K.; Fukuda, R.; Hasegawa, J.; Ishida, M.; Nakajima, T.; Honda, Y.; Kitao, O.; Nakai, H.; Vreven, T.; Montgomery, J. A., Jr.; Peralta, J. E.; Ogliaro, F.; Bearpark, M.; Heyd, J. J.; Brothers, E.; Kudin, K. N.; Staroverov, V. N.; Kobayashi, R.; Normand, J.; Raghavachari, K.; Rendell, A.; Burant, J. C.; Iyengar, S. S.; Tomasi, J.; Cossi, M.; Rega, N.; Millam, J. M.; Klene, M.; Knox, J. E.; Cross, J. B.; Bakken, V.; Adamo, C.; Jaramillo, J.; Gomperts, R.; Stratmann, R. E.; Yazyev, O.; Austin, A. J.; Cammi, R.; Pomelli, C.; Ochterski, J. W.; Martin, R. L.; Morokuma, K.; Zakrzewski, V. G.; Voth, G. A.; Salvador, P.; Dannenberg, J. J.; Dapprich, S.; Daniels, A.

https://dx.doi.org/10.1021/acs.joc.0c01124
J. Org. Chem. 2020, 85, 9808−9819

D.; Farkas, Ö.; Foresman, J. B.; Ortiz, J. V.; Cioslowski, J.; Fox, D. J.; Gaussian, Inc.: Wallingford CT, 2009.
(54) dos Passos Gomes, G.; Morrison, A. E.; Dudley, G. B.; Alabugin, I. V. Optimizing Amine-Mediated Alkyne−Allene Isomerization to Improve Benzannulation Cascades: Synergy between Theory and Experiments. *Eur. J. Org. Chem.* **2019**, *2019*, 512−518.
(55) Bickerton, G. R.; Paolini, G. V.; Besnard, J.; Muresan, S.; Hopkins, A. L. Quantifying the chemical beauty of drugs. *Nat. Chem.* **2012**, *4*, 90−98.
(56) Cremeens, M. E.; Hughes, T. S.; Carpenter, B. K. Mechanistic Studies on the Cyclization of (Z)-1,2,4-Heptatrien-6-yne in Methanol: A Possible Nonadiabatic Thermal Reaction. *J. Am. Chem. Soc.* **2005**, *127*, 6652−6661.
(57) Yu, M.; Liu, X.; Jiang, Q.; Du, H. Expeditious synthesis of 9-allenylpurines via cesium carbonate catalyzed isomerization of 9-alkynylpurines. *Phosphorus, Sulfur Silicon Relat. Elem.* **2018**, *193*, 451−458.
(58) Li, Y.; Chen, J.; Qiu, R.; Wang, X.; Long, J.; Zhu, L.; Au, C.; Xu, X. Cesium hydroxide-catalyzed isomerization of terminal alkynes for the synthesis of O-allenes and N-allenes. *Tetrahedron Lett.* **2015**, *56*, 5504−5507.
(59) Chen, W.; Li, J.; Zhu, Y.; Hu, W.; Moa, W. Et3N-promoted sequential reactions for the synthesis of 6H-benzo[c]chromenes. *ARKIVOC* **2012**, *6*, 16−25.
(60) Lyapunova, A. G.; Danilkina, N. A.; Rumyantsev, A. M.; Khlebnikov, A. F.; Chislov, M. V.; Starova, G. L.; Sambuk, E. V.; Govdi, A. I.; Bräse, S.; Balova, I. A. Relative Reactivity of Benzothiophene-Fused Enediynes in the Bergman Cyclization. *J. Org. Chem.* **2018**, *83*, 2788−2801.
(61) Kraka, E.; Cremer, D. Computer design of anticancer drugs. A new enediyne warhead. *J. Am. Chem. Soc.* **2000**, *122*, 8245−8264.
(62) Zhang, H.; Li, R.; Ba, S.; Lu, Z.; Pitsinos, E. N.; Li, T.; Nicolaou, K. C. DNA Binding and Cleavage Modes of Shishijimicin A. *J. Am. Chem. Soc.* **2019**, *141*, 7842−7852.
(63) Elmroth, K.; Nygren, J.; Mårtensson, S.; Ismail, I. H.; Hammarsten, O. Cleavage of cellular DNA by calicheamicin γ1. *DNA Repair* **2003**, *2*, 363−374.
(64) Hatayama, T.; Goldberg, I. H. DNA damage and repair in relation to cell killing in neocarzinostatin-treated HeLa cells. *Biochim. Biophys. Acta, Nucleic Acids Protein Synth.* **1979**, *563*, 59−71.
(65) Goodisman, J.; Kirk, C.; Dabrowiak, J. C. Kinetic analysis of drug cleavage of closed-circular DNA. *Biophys. Chem.* **1997**, *69*, 249−268.
(66) Freifelder, D.; Trumbo, B. Matching of single-strand breaks to form double-strand breaks in DNA. *Biopolymers* **1972**, *11*, 1116.
(67) Joyner, J. C.; Reichfield, J.; Cowan, J. A. Factors Influencing the DNA Nuclease Activity of Iron, Cobalt, Nickel, and Copper Chelates. *J. Am. Chem. Soc.* **2011**, *133*, 15613−15626.
(68) Zheng, Y. R.; Suntharalingam, K.; Johnstone, T. C.; Lippard, S. J. Encapsulation of Pt(IV) Prodrugs within a Pt(II) Cage for Drug Delivery. *Chem. Sci.* **2015**, *6*, 1189−1193.
(69) Dhar, S.; Lippard, S. J. Mitaplatin, a potent fusion of cisplatin and the orphan drug dichloroacetate. *Proc. Natl. Acad. Sci. U.S.A.* **2009**, *106*, 22199−22204.
(70) Chen, K.; Liao, S.; Guo, S.; Zhang, H.; Cai, H.; Gong, Q.; Gu, Z.; Luo, K. Enzyme/pH-sensitive dendritic polymer-DOX conjugate for cancer treatment. *Sci. China Mater.* **2018**, *61*, 1462−1474.
(71) Rankovic, Z. CNS Drug Design: Balancing Physicochemical Properties for Optimal Brain Exposure. *J. Med. Chem.* **2015**, *58*, 2584−2608.
(72) Lipinski, C. A.; Lombardo, F.; Dominy, B. W.; Feeney, P. J. Experimental and computational approaches to estimate solubility and permeability in drug discovery and development settings. *Adv. Drug Delivery Rev.* **1997**, *23*, 3−25.
(73) Rothkamm, K.; Barnard, S.; Moquet, J.; Ellender, M.; Rana, Z.; Burdak-Rothkamm, S. DNA damage foci: Meaning and significance. *Environ. Mol. Mutagen.* **2015**, *56*, 491−504.
(74) Chao, H. X.; Poovey, C. E.; Privette, A. A.; Grant, G. D.; Chao, H. Y.; Cook, J. G.; Purvis, J. E. Orchestration of DNA Damage Checkpoint Dynamics across the Human Cell Cycle. *Cell Syst.* **2017**, *5*, 445−459.e445.
(75) Pan, Z.; Luo, Y.; Xia, Y.; Zhang, X.; Qin, Y.; Liu, W.; Li, M.; Liu, X.; Zheng, Q.; Li, D. Cinobufagin induces cell cycle arrest at the S phase and promotes apoptosis in nasopharyngeal carcinoma cells. *Biomed. Pharmacother.* **2020**, *122*, No. 109763.
(76) Basel, Y.; Hassner, A. Imidazole and Trifluoroethanol as Efficient and Mild Reagents for Destruction of Excess Di-tert-butyl Dicarbonate [(BOC)2O]. *Synthesis* **2001**, *2001*, 0550−0552.

https://dx.doi.org/10.1021/acs.joc.0c01124
J. Org. Chem. 2020, 85, 9808−9819